

# PEEC Modelling of Toroidal Magnetic Inductor in Frequency Domain

I. F. Kovačević, A. Müsing, and J. W. Kolar

Power Electronic Systems Laboratory, ETH Zurich, Physikstrasse 3, 8092 Switzerland  
kovačević@lem.ee.ethz.ch

**Abstract**—In this paper, a detailed 3D Partial Element Equivalent Circuit (PEEC) model of a toroidal coil with a magnetic core is developed. The PEEC problem in the presence of magnetic materials is solved in the frequency domain via a magnetic current/charge approach, i.e. replacing the magnetized objects by a distribution of equivalent fictitious magnetic currents/charges in free space. The simulation parameters are the winding and magnetic core properties. The permeability is either taken from datasheets or determined by measuring the series equivalent impedance. To verify the proposed 3D PEEC model, calculated and measured impedance values are compared for several winding arrangements and core materials. A good agreement between simulation and measurements is presented up to the first resonant frequency. For higher frequencies, a more accurate specification of the permeability is required, as well as the core dielectric property has to be considered.

**Index Terms**—Complex permeability, magnetic currents and charges, toroidal core inductor, PEEC.

## I. INTRODUCTION

Due to increasing switching frequency and higher power density of converter systems, power electronics engineers deal with significant electromagnetic interference problems that have to be considered in the earliest system design stage. To comply with EMC standards, the conducted and radiated emission levels generated by power electronic (PE) systems have to be controlled, necessitating employment of EMI filter circuits. Accordingly, EMI filter components have to be considered, including their high frequency behaviour in combination with PCB placement and parasitic couplings. There, an optimized arrangement of filter components is required to fulfil legal EMI specifications with minimum realization effort.

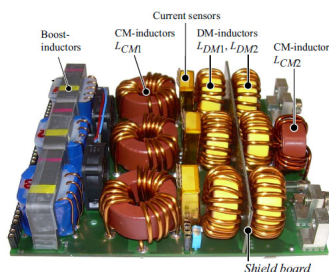


Fig. 1. Example of an input filter of a three-phase PWM rectifier [1].

The selection of the basic building blocks i.e. inductors and capacitors, for an optimal EMI filter (see Fig. 1), requires a comprehensive analysis of both component

characteristics and their mutual EM coupling to other components in order to obtain correct filter attenuation at higher frequencies. As the volume of power converter systems decreases, the placement of components becomes a critical issue. Also, as a result of parasitic effects, the passive components can change their characteristics considerably at higher frequencies, and together with the mutual electromagnetic coupling, the EMI performance of the overall PE system can be significantly degraded. To illustrate the influence of parasitic effects and mutual coupling, a passive T-network employed in low-pass EMI filtering ( $L_1$ ,  $L_2$ ,  $C_p$ ) and its equivalent circuit are presented in Fig. 2.

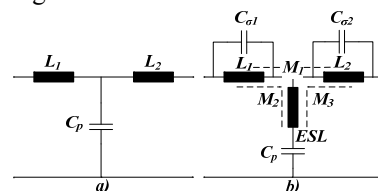


Fig. 2. Passive T-network employed in low-pass EMI filtering: (a) filter circuit, (b) the equivalent circuit showing the parasitic elements.

The capacitance  $C_{\sigma 1}$  and  $C_{\sigma 2}$  are the parasitic self capacitances of the inductors  $L_1$  and  $L_2$ , while  $ESL$  is the equivalent parasitic series self inductance of the filter capacitor  $C_p$ . The mutual inductances  $M_{1,3}$  are used to model the magnetic couplings. The effect of coupling on the performance of this filtering stage is an effective alternation of  $L_1$ ,  $L_2$  and  $ESL$  e.g. the equivalent inductance  $L_1$  due to coupling is  $L_{1,eq} = L_1 + M_1 + M_2 + M_3$  [2]. Also, the parallel capacitance  $C_{\sigma 1}$  and  $C_{\sigma 2}$  decrease the filter attenuation at higher frequencies and determine resonant frequencies above which the inductors  $L_1$  and  $L_2$  become predominantly capacitive. It has been shown that the influence of these effects cannot be neglected and has to be modelled in order to determine the real behaviour of the overall design [3]. Accordingly, accurate simulation techniques are required in the design process of power electronic systems.

As illustrated in Fig. 1, the main components of an EMI filter are toroidal inductors which are preferred due to their geometry i.e. closed uninterrupted magnetic path and constant cross section, and their magnetic properties i.e. highest effective permeability [4]. In this paper, a 3D comprehensive EM modelling approach of toroidal magnetic inductors based on the Partial Element Equivalent Circuit (PEEC) method is developed. The PEEC is also used as a tool for EM modelling of inductive behaviour including the mutual coupling mechanism and parasitic effects. The aim of the presented

research is to simulate the low- and high- frequency EM behaviour of magnetic inductors. The geometry of interest is a coil wrapped around the toroidal magnetic core with rectangular cross section. According to EMC regulations and standards, the frequency range of interest is from 150 kHz to 30 MHz.

In **Section II**, the capabilities of the PEEC method are described and compared to other EM simulation techniques like the Finite Element Method (FEM) and the Method of Moments (MoM). **Section III** gives a brief overview of prior research in the field of PEEC modelling in the presence of magnetic material. **Section IV** describes the theory of the magnetic current and magnetic charge approaches and in **Section V**, the PEEC interpretation of Maxwell's equations in the presence of magnetic materials and the integration of the PEEC and the Boundary Element (BE) methods are presented. Finally in **Section VI**, in order to verify the proposed PEEC simulation, coil impedance measurements in the frequency range from 40 Hz up to 110 MHz are performed and compared to the PEEC simulation results. The conclusions in **Section VII** summarize the final results and point to the topics of further research.

## II. PEEC - EM SIMULATION TOOL

The Partial Element Equivalent Circuit (PEEC) method has proven to be a fast and accurate simulation method for calculating parasitic layout effects of power converters [5]. PEEC modelling dates from the 1970s when the work of Ruehli established the basis of today's PEEC approach, as an integral formulation of Maxwell's equations and their interpretation in terms of partial circuit elements [6]. The PEEC method covers both time and frequency domain and takes into account capacitive and inductive couplings all together. It can be used to model skin and proximity effects, and has the ability to solve EM problems with significantly less computational effort than the Finite Element Method (FEM), which is in turn based on the differential formulation of Maxwell's equations. Compared to FEM, the PEEC method does not require meshing of the whole volume space (plus surrounding air), but only of the volume of conductors, and/or dielectric or magnetic components. Therefore it is useful especially for open-air problems. What distinguishes PEEC from other integral EM formulations, such as the Method of Moments (MoM), is that it is a full-wave method valid from DC to high frequency. Additionally, due to its circuit description and its capability of a subsequent model order reduction, PEEC models can be integrated easily into standard circuit solvers.

The main difficulty of the PEEC method is the PEEC interpretation of Maxwell's equations for inhomogeneous environments e.g. dielectric and magnetic regions. So far, dielectrics have been successfully integrated into PEEC solvers [7], while the main drawback is the incapability to apply the standard PEEC method in the presence of inhomogeneous, nonlinear magnetic materials. For this class of EM problems, the FEM method is so far the method of choice.

As magnetic materials have the ability to change the external electromagnetic field, an adequate modification of the electric field Maxwell's integral equations (EFIE) is required in order to keep the structure of PEEC equations suitable for circuit description. According to electromagnetic field theory, two approaches to model the EM influence of a magnetic medium exist: the equivalent magnetic current method and the equivalent magnetic charge method. Namely, the problem of the calculation of the magnetic field in the presence of magnetic materials can be simplified by replacing the magnetized objects by an equivalent distribution of bounded currents or by an equivalent distribution of fictitious magnetic charges [8].

From the aspects of building a fast power electronic EMI simulator, the main challenge is to determine the PEEC models of the magnetic elements like coils, sensors, inductors, transformers, etc. which are the standard components of power electronics systems like EMI filters, power converters, and electrical machines. The simulation under the justified approximations should correspond well to the real performance of the component over a wide frequency range, taking into account also mutual inductive and capacitive couplings. However, PEEC models of standard magnetic geometries do not yet exist.

## III. LITERATURE SURVEY

Several works found in literature describing the PEEC modelling of linear magnetic materials can be classified to the magnetic current approach [9]-[11]. In [9], the theoretical basis and the calculation of PEEC coefficients for the basic geometries like wire, dipole, sheet, and slab were presented. In [10], an extension to the PEEC method called  $\mu$ PEEC was introduced, and verified on two academic examples. In [11], a software tool for RF IC inductor designs based on the so-called magPEEC was developed, which it is another extension to the PEEC approach to analyze arbitrary conductor-magnetic structures.

Another method, essentially different from the magnetic current/charge approach, was developed in [12], [13] which is based on the assumption that the direction of stray field produced by a magnetic inductor is not influenced by its constitutive ferromagnetic magnetic material. This method is applicable for the modelling of common mode inductors in EMI filters where the leakage field is generated by DM currents and the leakage inductance can be calculated by means of the effective permeability constant  $\mu_{\text{eff}}$ , which depends for highly permeable materials only on the geometry. Specifically, the PEEC equivalent circuit considering the magnetic materials is built by adding a current and a voltage source and adapting the values of the PEEC air-mutual inductances by  $\mu_{\text{eff}}$ . This approach does not take into account the 3D structure of the toroidal coil, is valid only for highly permeable materials and not applicable for general arbitrary shaped magnetic geometry.

In [14], a hybrid 3D PEEC-FEM coupled method was presented. The FEM-PEEC coupling is employed to use

the advantage of both differential and integral formulations where FEM is applied for modelling magnetic materials and PEEC for conductors. By such an approach, the problem of a complex FEM mesh is not fully avoided but is lessened in the way that the mesh around conductors is relaxed.

The aim of this paper is to comprehensively model toroidal magnetic inductors and to investigate a general PEEC approach for modelling the mutual coupling mechanisms and the characteristics of the standard PE magnetic components.

#### IV. EM FIELD THEORY OF MAGNETIC MATERIALS

While a dielectric medium modifies the electric field, a magnetic medium has influence on the magnetic field produced by surrounding field sources. A magnetic material is characterized by the magnetization vector  $\mathbf{M}$ . The contribution of a magnetic volume  $V_m$  to the total magnetic field can be described either by the magnetic vector potential  $\mathbf{A}_M$  [15],

$$\mathbf{A}_M(\mathbf{r}) = \frac{\mu_0}{4\pi} \int_{V_m} \frac{\nabla_{\mathbf{r}_m} \times \mathbf{M}(\mathbf{r}_m)}{|\mathbf{r} - \mathbf{r}_m|} dV_m + \frac{\mu_0}{4\pi} \oint_{S_m} \frac{\mathbf{M}(\mathbf{r}_m) \times \mathbf{n}(\mathbf{r}_m)}{|\mathbf{r} - \mathbf{r}_m|} dS_m, \quad (1)$$

or the magnetic scalar potential  $V^{(M)}$  (2),

$$V^{(M)}(\mathbf{r}) = \frac{1}{4\pi} \int_{V_m} \frac{-\nabla_{\mathbf{r}_m} \cdot \mathbf{M}(\mathbf{r}_m)}{|\mathbf{r} - \mathbf{r}_m|} dV_m + \frac{1}{4\pi} \oint_{S_m} \frac{\mathbf{M}(\mathbf{r}_m) \cdot \mathbf{n}(\mathbf{r}_m)}{|\mathbf{r} - \mathbf{r}_m|} dS_m \quad (2)$$

where  $\mathbf{r}$  and  $\mathbf{r}_m$  are the positions of the field point and of an elementary magnetic volume source,  $S_m$  is the surface of the magnetic volume  $V_m$ , and  $\mathbf{n}(\mathbf{r}_m)$  is the unit vector pointing outwards normal to  $S_m$  at the magnetic point  $\mathbf{r}_m$ . Using magnetic potentials, it can be shown that the influence of magnetization  $\mathbf{M}$  in the volume  $V_m$  to the total magnetic field at any point in space is equivalent to the influence of a “fictitious magnetic current” or a “fictitious magnetic charge” distribution existing within the material boundary  $V_m$  characterized by the permeability of free space  $\mu_0$ .

##### A. Magnetic Current and Magnetic Charge Approaches

The magnetic current approach is derived from (1). Equation (1) can be interpreted as the magnetic vector potential generated by a volume current density  $\mathbf{J}_m$  inside of the volume  $V_m$  and a surface current density  $\mathbf{K}_m$  at the magnetic surface  $S_m$ ,

$$\mathbf{J}_m = \nabla_{\mathbf{r}_m} \times \mathbf{M}(\mathbf{r}_m), \quad \mathbf{K}_m = \mathbf{M}(\mathbf{r}_m) \times \mathbf{n}(\mathbf{r}_m). \quad (3)$$

By nature, the currents  $\mathbf{J}_m$  and  $\mathbf{K}_m$  are bounded fictitious currents in the free space known as “Amperian” currents.  $\mathbf{J}_m$  and  $\mathbf{K}_m$  influence the magnetic field but do not generate a voltage drop along the magnetic volume or its surface. The magnetic induction  $\mathbf{B}_M$  can be calculated in the same way as the magnetic induction  $\mathbf{B}$  of the free electrical currents  $\mathbf{J}_e$  and  $\mathbf{K}_e$ , setting  $\mathbf{J}_e = \mathbf{J}_m$  and  $\mathbf{K}_e = \mathbf{K}_m$ ,

$$\mathbf{B}_M(\mathbf{r}) = \frac{\mu_0}{4\pi} \left[ \int_{V_m} \frac{\mathbf{J}_m(\mathbf{r}_m) \times (\mathbf{r} - \mathbf{r}_m)}{|\mathbf{r} - \mathbf{r}_m|^3} dV_m + \int_{S_m} \frac{\mathbf{K}_m(\mathbf{r}_m) \times (\mathbf{r} - \mathbf{r}_m)}{|\mathbf{r} - \mathbf{r}_m|^3} dS_m \right]. \quad (4)$$

The magnetic charge approach is derived from (2). Similar to the previous analysis, the magnetic medium

can be replaced by bounded, fictitious magnetic charges,

$$\rho_m(\mathbf{r}_m) = -\nabla_{\mathbf{r}_m} \cdot \mathbf{M}(\mathbf{r}_m), \quad \sigma_m(\mathbf{r}_m) = \mathbf{M}(\mathbf{r}_m) \cdot \mathbf{n}(\mathbf{r}_m) \quad (5)$$

which produce the same magnetic scalar potential as the magnetization vector  $\mathbf{M}$  so that magnetic field strength  $\mathbf{H}_M$  can be calculated by

$$\mathbf{H}_M(\mathbf{r}) = \frac{1}{4\pi} \left[ \int_{V_m} \frac{\rho_m(\mathbf{r}_m)(\mathbf{r} - \mathbf{r}_m)}{|\mathbf{r} - \mathbf{r}_m|^3} dV_m + \oint_{S_m} \frac{\sigma_m(\mathbf{r}_m)(\mathbf{r} - \mathbf{r}_m)}{|\mathbf{r} - \mathbf{r}_m|^3} dS_m \right]. \quad (6)$$

The influence of magnetic charges to the surrounding magnetic field is expressed by (6).

##### B. Special Cases

For uniformly magnetized and linear homogeneous magnetic materials  $\rho_m$  and  $\mathbf{J}_m$  are zero. Then, the internal magnetic volume has no contribution to the total magnetic field, so that only the surface of the magnetic body needs to be modeled. Linearity is described by the permeability  $\mu_r$  or the magnetic susceptibility  $\chi_m = \mu_r - 1$ . The typically used magnetic cores, i.e. powder, ferrite, and amorphous cores, are characterized by their permeability coefficients  $\mu_r$ . As the real behaviour of magnetic materials varies with frequency  $f$  and magnetic field  $H$ ,  $\mu_r$  is defined as a function of these variables rather than as constant value. The instantaneous characteristics of magnetic materials can be well approximated by  $\mu_r(f, H)$ . Some core manufacturers provide the corresponding detailed permeability curves in their datasheets.

#### V. COUPLING PEEC AND BOUNDARY ELEMENT METHOD

In the previous Section it is shown that regarding the calculation of magnetic field, an object with magnetic characteristics can be replaced with either an equivalent current or an equivalent charge density distribution. These currents or charges can be then seen as new sources of the magnetic field, implying that a modification of Electric Field Integral Equation (EFIE) is needed for PEEC EM modelling.

For small toroidal cores with highly resistive magnetic material, the influence of induced eddy currents within the magnetic core can be neglected. It has also been shown in [16] that the power losses due to hysteresis and residual losses are in general much lower than copper losses. Therefore, regarding electrical behaviour, it is justifiable to set the free electric currents within the core to zero alleviating the modelling problem, and only the equivalent magnetic surface quantities, namely currents and charges, are taken into account. Core losses can be included by the value of complex permeability

$$\bar{\mu} = \mu' - j\mu'' \quad (7)$$

The real part of the complex permeability  $\mu'$  describes the enhancement of inductance in comparison to an air-core inductor and the imaginary part of permeability  $\mu''$  describes losses and the phase shift between the incident field and the flux within the core [17]. The influence of the dielectric properties of magnetic cores is discussed in Section VI.

A toroidal coil with its windings equally distributed over the entire core surface and high  $\mu_r$  has a very low magnetic stray field so that the magnetic field lines are almost tangential to the magnetic path. This means that in an ideal case no magnetic charge exists

$$\sigma_m(\mathbf{r}_m) = \mathbf{M}(\mathbf{r}_m) \cdot \mathbf{n}(\mathbf{r}_m) = M_n(\mathbf{r}_m) = \chi_m H_n(\mathbf{r}_m) = 0. \quad (8)$$

Accordingly, the influence of the core, i.e. the increase of the main magnetic flux density within the coil, has to be described by means of equivalent magnetic surface currents. On the other hand, the fictitious magnetic charges contribute to the stray field of the inductor as it was shown in [18] on the example of transformer leakage inductance.

In the first approximation, the simplified permeability characteristic  $\mu_r = \mu_r(f)$  is used. For an impedance analysis by measurement, the DC bias is usually zero or less than 100 mA so that  $\mu_r$  is equal to the initial permeability. During a measurement, the inductor is observed as a separate component and no external mutual couplings are present. Further research tasks will be to include the non-linear properties of the core material described by  $B$ - $H$  hysteresis characteristic. As the operating point moves across the  $B$ - $H$  curve i.e. the DC bias changes, the permeability varies in time and  $\mu_r(H)$  needs to be considered e.g. boost inductors of PFC rectifiers and DM inductors. Modeling of non-linear core characteristics in frequency domain becomes difficult and a time-domain model appears more convenient, but then the modeling problem of core losses defined by  $\mu$  arises.

#### A. PEEC Electric Field Integral Equation (EFIE)

The analyzed modeled geometry is presented in Fig. 3. The modification of the PEEC equations for the case of the magnetic current approach is derived in [9]. The surface of the toroidal core is discretized into  $N_M$  panels carrying ‘‘Amperian’’ currents  $\mathbf{K}_{mi}$ , ( $mi = 1 \dots N_M$ ). The magnetic surface current has two components, in  $\theta$ - and  $\varphi$ - directions, respectively  $K_{mi,\theta}$  and  $K_{mi,\varphi}$ . The  $K_{mi,\varphi}$  currents produce the axial flux within the core while the  $K_{mi,\theta}$  currents originate from the stray magnetic field i.e. field lines going out of the core.

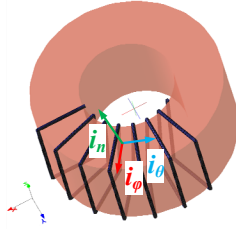


Fig. 3. The modeled geometry of a toroidal magnetic inductor with non-uniform winding arrangement.

The coil with  $N_J$  turns is modeled by  $4N_J$  cylindrical volume sub-cells where a turn is approximated as a PEEC volume cell consisting of four connected cylindrical volume sub-cells. Therefore, two PEEC nodes correspond to one turn i.e. in the case of a winding on a magnetic core, the number of electrically equivalent PEEC nodes is equal to  $N_S = N_J + 1$ . The coil and the  $K_{mi,\varphi}$  currents are

descriptively represented in Fig. 4.

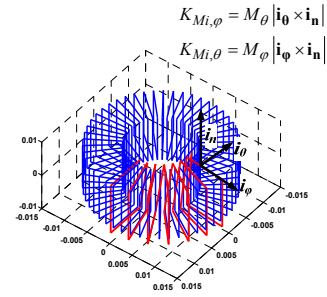


Fig. 4. The  $K_{mi,\varphi}$  surface magnetic currents (blue) and the coil (red) on the toroidal magnetic inductor:  $K_{mi,\varphi}$  form rectangular loops while coil currents form a spiral around the core.

Consequently, in the presence of magnetic material, the order of the PEEC system matrix increases. The unknowns are the winding currents  $\mathbf{I}$ , the voltages of the PEEC nodes  $\mathbf{V}$ , and the magnetic surface currents  $\mathbf{K}_m$ . If the  $k$ -th ( $k = 1 \dots N_J$ ) electric PEEC volume cell i.e.  $k$ -th turn, is observed, the simplified ordinary PEEC EFIE can be rewritten as (9) [9]. The EFIE is extended by the matrices  $\mathbf{L}_{K_m\varphi}$  and  $\mathbf{L}_{K_m\theta}$  consisting of additional partial elements i.e. the mutual inductances between the fictitious surface magnetic currents  $K_{mi}$  ( $mi = 1 \dots N_M$ ) and the winding currents  $I_i$  ( $i = 1 \dots N_J$ ).

$$V_n = R_n I_n + \sum_{i=1}^{N_J} L_{in} \frac{dI_i}{dt} + \sum_{i=1}^{N_S} Q_i [pp_{in}^+ - pp_{in}^-] + \dots + \sum_{mi=1}^{N_M} L_{K_{mi,\varphi},n} \frac{dK_{mi,\varphi}}{dt} + \sum_{mi=1}^{N_M} L_{K_{mi,\theta},n} \frac{dK_{mi,\theta}}{dt}. \quad (9)$$

According to (5) and (6), another way to model the stray field is by means of the fictitious magnetic charges  $\sigma_{mi}$  ( $mi = 1 \dots N_M$ ) set on the  $N_M$  magnetic panels. Introducing the fictitious magnetic charges instead of  $K_{mi,\theta}$  surface currents, the EFIE can be represented by

$$V_n = R_n I_n + \sum_{i=1}^{N_J} L_{in} \frac{dI_i}{dt} + \sum_{i=1}^{N_S} Q_i [pp_{in}^+ - pp_{in}^-] + \dots + \sum_{mi=1}^{N_M} L_{K_{mi,\varphi},n} \frac{dK_{mi,\varphi}}{dt} + \sum_{mi=1}^{N_M} L_{\sigma_{mi},n} \frac{d\sigma_{mi}}{dt}. \quad (10)$$

The matrix  $\mathbf{L}_{\sigma M}$  represents the mutual magnetic coupling effect between the magnetic panels carrying the fictitious magnetic charges  $\sigma_{mi}$  ( $mi = 1 \dots N_M$ ) and the winding currents ( $I_i$ ,  $i = 1 \dots N_J$ ). According to (6), the magnetic charges are seen as additional sources producing a voltage drop in the winding turns i.e. the fifth term of (10).

The equivalent PEEC circuit of a magnetic inductor is presented in Fig. 5. Finally, the simulated impedance of an inductor is then calculated as  $Z_L = V_I / I_{IN}$ .

#### B. Integration of PEEC and Boundary Element Method

The correlation between surface currents and the winding currents is derived by the boundary element (BE) method. According to Maxwell's electromagnetic theory, as boundary conditions the continuity of the tangential component  $H_t$  and of the normal component

$B_n$ , have to be satisfied at the interface between two different mediums. If the magnetic field is derived from the magnetic vector potential, the continuity of  $B_n$  is automatically enforced by (1) and the continuity of  $H_t$  has to be set. For magnetic scalar potential, the opposite conditions are applied respectively.

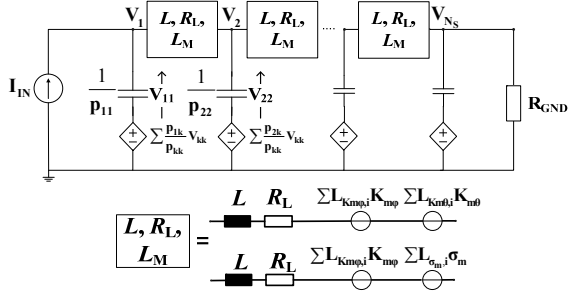


Fig. 5. The PEEC equivalent circuit for a magnetic inductor.

In the case of the magnetic current approach, the BE equation for the  $mk$ -th magnetic panel ( $mk = 1 \dots N_M$ ) is given by [19],

$$\left(\frac{\mathbf{B}_{\mathbf{J}(mk)}}{\mu_0} + \frac{\mathbf{B}_{\mathbf{M}(mk)}}{\mu_0}\right) \times \mathbf{n}_{mk} - \left(\frac{1}{2} + \frac{1}{\chi_m}\right) \mathbf{K}_{mk} = 0 \quad (11)$$

$$\Rightarrow \lambda_{\text{MI}} \cdot \mathbf{I} + \alpha_{\text{MM}} \cdot \mathbf{K}_{\mathbf{M}} = 0,$$

where  $\mathbf{n}_{mk}$  is the unit vector pointing outwards normal to the  $mk$ -th magnetic panel,  $\mathbf{B}_{\mathbf{J}(mk)}$  is the magnetic induction of the coil and  $\mathbf{B}_{\mathbf{M}(mk)}$  is the magnetic induction of other magnetic panels ( $mi \neq mk$ ) calculated at the  $mk$ -th magnetic panel. The same terminology as in [9] is used for naming the new matrices  $\alpha$  and  $\lambda$ . The problem of singularity arises with the calculation of  $\alpha_{mk,mk}$ , i.e. the influence of the  $mk$ -th magnetic panel to itself. Although the discretization has an influence on the final results, the calculated singularity (the term  $\alpha_{mk,mk} = +1/2$ ) in (11) does not depend on the panel size. The modification of  $\alpha_{mk,mk}$  is needed in order to obtain correct simulation results. Therefore, to reduce the computational error, the cancellation of the permeability free terms is enforced [20].

The standard PEEC system matrix [21] is then refilled with new elements  $L_M$ ,  $\lambda_{MI}$ , and  $\alpha_M$ , leading to the PEEC system matrix for a toroidal magnetic inductor,

$$\begin{bmatrix} \mathbf{A} & -(\mathbf{R} + j\omega \mathbf{L}) & -j\omega \mathbf{L}_M \\ (j\omega \mathbf{P}^{-1} + \mathbf{Y}_L) & \mathbf{A}^T & 0 \\ 0 & \lambda_{\text{MI}} & \alpha_{\text{MM}} \end{bmatrix} \begin{bmatrix} \mathbf{V} \\ \mathbf{I} \\ \mathbf{K}_M \end{bmatrix} = \begin{bmatrix} \mathbf{V}_S \\ \mathbf{I}_S \\ \mathbf{0} \end{bmatrix} \quad (12)$$

The standard PEEC matrix is defined by the connectivity matrix  $\mathbf{A}$ , the resistance and inductance matrices of electric PEEC cells  $\mathbf{R}$  and  $\mathbf{L}$ , the matrix of potentials  $\mathbf{P}$  and by the admittance matrix  $\mathbf{Y}_L$ . In the first modeling stage, the matrix  $\mathbf{P}$  includes only the winding capacitance i.e. turn-to-turn capacitances.

By analogy, if the fictitious magnetic charges are introduced, the boundary equation,

$$(\mathbf{H}_{\mathbf{J},mk} + \mathbf{H}_{\mathbf{M},mk}) \cdot \mathbf{n}_{mk} - \left(\frac{1}{2} + \frac{1}{\chi_m}\right) \sigma_{mk} = 0 \quad (13)$$

$$\Rightarrow \lambda_{\text{qMI}} \cdot \mathbf{I} + \gamma_{\text{MM}} \cdot \sigma_{\mathbf{M}} = 0,$$

has to be satisfied and the PEEC system matrix for a magnetic inductor is defined by,

$$\begin{bmatrix} \mathbf{A} & -(\mathbf{R} + j\omega \mathbf{L}) & -j\omega \mathbf{L}_M \\ (j\omega \mathbf{P}^{-1} + \mathbf{Y}_L) & \mathbf{A}^T & 0 \\ 0 & \lambda_{\text{qMI}} & \gamma_{\text{MM}} \end{bmatrix} \begin{bmatrix} \mathbf{V} \\ \mathbf{I} \\ \sigma_{\mathbf{M}} \end{bmatrix} = \begin{bmatrix} \mathbf{V}_S \\ \mathbf{I}_S \\ \mathbf{0} \end{bmatrix} \quad (14)$$

The order of the system matrix is then increased by  $2N_M$  that is the number of additional unknowns, magnetic surface currents and/or charges.

## VI. MEASUREMENTS VS. PEEC SIMULATION RESULTS

To verify the proposed PEEC simulation approach, experimental measurements of impedance characteristics of several inductors are compared to the PEEC simulation results for different core types and uniform (U) and non-uniform (NU) winding arrangements. The measurements are performed by means of an Agilent 4294A impedance analyzer, operating in the range from 40 Hz up to 110 MHz. Three different magnetic materials are selected: nanocrystalline VITROPERM 500F, ferrite T38 and molypermalloy powder (MPP). Details about the analyzed magnetic inductors are given in Table I. VITROPERM 500F and ferrites are typically used for CM filter inductors as they are characterized by high initial permeability respectively up to  $10^5$  and  $10^4$  [22], [23]. On the other hand, MPP powder cores have considerably lower permeability but as distributed air gap cores, they exhibit high saturation flux density which makes them convenient for DM filter inductors [24].

### A. PEEC Simulation Parameters

The simulation inputs are the permeability characteristics of the magnetic core and the winding properties. In the measurement conditions,  $\mu_r$  is equal to the initial permeability which in turn changes only with frequency. For the simulation, the  $\mu_r(f)$  is taken from the core datasheet or calculated from measurements.

It has to be pointed out that the critical input parameter for the PEEC simulation is the permeability characteristic of the core material. Depending on the application, the datasheets provide either the complex permeability vs. frequency  $\mu'(f)$  and  $\mu''(f)$  or the effective relative permeability vs. frequency  $\mu_r(f)$ . In the conventional complex permeability measurements, the series inductance  $L_s$  and resistance  $R_s$  of the inductor are measured at different frequencies. Subsequently,  $L_s$  and  $R_s$  are recalculated into  $\mu'$  and  $\mu''$  [17].

For ferrites characterized by higher relative permittivity  $\epsilon$  ( $= \epsilon' - j\epsilon''$ ), the manufacturers measure permeability characteristics on smaller size ring cores e.g. R10, to avoid dimensional effects [25], [26]. Accordingly, the permeability curves from datasheets do not correctly describe the intrinsic permeability of cores with different dimensions. As a result of pronounced dielectric properties, the induced displacement currents can change the field within the core and considerably change the behavior of inductor. At higher frequencies, the imaginary part  $\epsilon''$  is responsible for reduction of the incident field in the core, what is not included in the

proposed PEEC model at the current development stage.

The data provided by the manufacturer could deviate from the actual behavior by 20-30% and the permeability characteristics can be statistically determined by measuring several cores with same dimensions. In addition, the influence of the winding arrangement can significantly alter permeability measurement results at higher frequencies [27], so special care must be taken concerning the number of turns and the winding arrangement. For EMI filter inductors, typically a single-layer winding is employed to reduce parasitic capacitance.

All these issues were observed in the impedance measurements of different inductors (Table I). Namely, the standard inductance measurements are performed with the awareness that measurements provide information only about the permeability properties of material at lower frequencies, at higher frequencies they contain the influence of winding and/or dimensional effects. As a result, the frequency range of interest can be divided into lower and higher frequency regions defined by a frequency  $f_i$  as shown in Fig. 6.

The frequency  $f_i$  depends on the winding arrangement and the core magnetic properties as it is shown in the following section.

TABLE I  
THE INFORMATION ABOUT THE ANALYZED MAGNETIC INDUCTORS.

	Manufacturer	Material/ Core Size	Winding/ Turns	Wire Diam.
1	Vacuumschmelze	VITROPERM/ W380	U / 7	1.5mm
2	Vacuumschmelze	VITROPERM/ W380	U / 20	0.5mm
3	EPCOS	Ferrite T38/R34.0	NU / 3	1.5mm
4	EPCOS	Ferrite T38/ R34.0	NU / 20	1.5mm
5	EPCOS	Ferrite T38/ R34.0	U / 30	1.5mm
6	Micrometals	MPP-26/ R27.9	U / 22	1.5mm

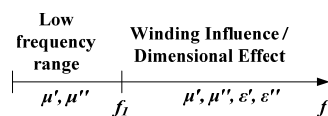


Fig. 6. The frequency ranges for permeability measurements in which different effects can be observed ( $f_i$  = the first resonant frequency).

### B. PEEC Simulation Results

The effective relative permeability curves of some magnetic materials, e.g. MPP-26 are described in Bode-plots as linear functions that can be easily implemented in the PEEC frequency domain simulation [2]. Using the effective permeability for simulation i.e. ignoring the core losses (example 6 in Table I), a good agreement between the measurements and the simulation can be observed in the first frequency range (Fig. 6) up to  $f_i$  which coincides with the resonant frequency for Micrometals MPP-26 core (Fig. 7). The impedance at the resonant frequency is determined by the winding capacitance resulting from turn-to-turn capacitance included in the PEEC model and other factors such as

core resistance and core-winding capacitance which are not directly considered in the PEEC simulation. However, in the frequency range of the interest below the resonant frequency, the PEEC simulation provides the information useful for the design and the modeling of an inductor.

To further analyze the results of the PEEC simulation, an experiment is conducted based on the measurements for two/three inductors with same core material but different windings (examples 1-5 in Table I). For permeability measurement, the inductor which exhibits the smallest influence of windings is chosen and the other inductors are used for the verification of the PEEC modeling approach. Nanocrystalline VITROPERM 500F (examples 1) and ferrite T38 (example 3) core materials are used for the measurements.

The experiment with a nanocrystalline VITROPERM 500F magnetic core is conducted using windings with seven and twenty turns and different wire diameters (see Table I). The permeability curves are extracted from the impedance measurements of the winding with seven turns uniformly distributed around the core (Fig. 8). Using these curves as inputs, the impedance of the 20 turns inductor is simulated and the results are presented in Fig. 9. A good agreement between the measurements and the simulation is observed up to the first resonant frequency. At higher frequencies, the small differences result from the capacitive influence captured in the measured permeability curves.

Similarly, the measurement is conducted for a ferrite T38 core, so that permeability curves are extracted from the impedance measurements of the 3 turns inductor (Fig. 10) and used for the simulation of the 20 turns and 30 turns inductors. From the permeability curves (Fig. 10), it can be seen that at the frequency around 2 MHz, the inductor with only three turns starts behaving capacitively i.e. the real part of complex permeability is negative. Such a behavior results from the high dielectric properties of ferrites, high permittivity of core  $\epsilon \approx 2 \cdot 10^5$  [25], [26]. Hence, the simulation results comply with the measurements in the frequency range up to  $f_i \approx 2\text{MHz}$  (Fig. 11 and Fig. 12).

### C. PEEC Simulation Analysis

The 3D PEEC modeling approach of a magnetic toroidal inductor provides not only the inductor impedance but it can also accurately explain the real behavior of inductor at higher frequencies. Solving the PEEC system matrix, it is shown that the current is not evenly distributed in turns at higher frequencies due to the turn-ground capacitance i.e. self-capacitance calculated by the coefficients of potentials defining the potential matrix  $\mathbf{P}$ .

Analyzing the influence of the terms in (9) and (10), it is shown that the simulation results agreed with the current distribution presented in Fig. 4. The surface currents  $\mathbf{K}_{M\phi}$  form current loops and hence do not produce a significant change of the magnetic field outside of the inductor, while the surface currents  $\mathbf{K}_{M\theta}$  have few orders lower amplitude and do not significantly influence the inductance calculation. Consequently, the impedance

is primarily determined by the surface currents  $\mathbf{K}_{M\theta}$ , and the surface currents  $\mathbf{K}_{M\theta}$  or the surface magnetic charges  $\sigma_M$  can be used to calculate the external effect due to the presence of magnetic core. This fact implies an idea for simulating other magnetic core geometries e.g. E-cores. The core material can be replaced by a magnetic surface current distribution of the same geometric shape as the core producing the magnetic flux within the core defined by the equivalent magnetic circuit of the inductor. Simultaneously, the coupling effect in the presence of magnetic material can be explained by existence of magnetic surface charges producing the additional external field.

D. Future Research

In future research several topics have to be examined in more detail: (1) simulation of the mutual coupling mechanism to validate the assumptions in [13] that the stray EM field is not significantly influenced by the magnetic core, (2) dielectric properties of magnetic cores and more accurate permeability measurement methods [27], (3) inductors with multilayered windings, (4) E-core geometry modeling and (5) parasitic coupling effects between EMI filter components. As for ferrites the core dielectric properties take effect already around a few MHz, the winding-core capacitance will be also included in the PEEC model taking the permittivity of core as a simulation parameter.

VII. CONCLUSIONS

In this paper, a 3D PEEC model of a magnetic toroidal inductor with rectangular cross section in the frequency domain is developed. The presence of magnetic core is simulated by replacing the toroidal core with equivalent distributions of fictitious magnetic charges and currents on the core surface. To correlate magnetic currents/charges with the induced electrical currents, the boundary element method is employed.

It is shown that magnetic currents producing the axial field deterministically effect the inductance calculation and do not have significant influence on the coupling to neighboring components. On the other hand, the coupling in the presence of magnetic material can be explained by influence of fictitious magnetic charges. According to these results, the PEEC/BE modeling of different magnetic core geometries like E-cores is also possible.

To verify the proposed PEEC method, the simulated and measured inductances are compared for different winding arrangements and core materials. A good agreement between the measurements and the PEEC simulation is observed below the first resonant frequency. It is shown that the critical simulation input parameter is the complex permeability and that dielectric properties can take effect in the low-loss frequency range around approximately 1-2 MHz. Therefore, the permittivity has to be included as a simulation parameter for the magnetic cores with strong dielectric properties such as ferrite cores. To improve the modeling, the dielectric and magnetic properties of magnetic cores have to be measured with more accurate techniques. Additionally,

an approach for the PEEC modeling of core-winding capacitance will be investigated i.e. setting the bounded charges onto the surface of the core such that the BE equation for the continuity of electric field tangential component is satisfied. The presented PEEC/BE method enables the modeling of the parasitic and mutual coupling mechanisms. The time domain simulation will be also investigated in future.

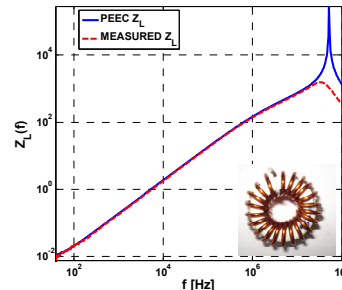


Fig. 7. Comparison of the impedance of the PEEC modeled inductor with the measurements (Micrometals T94-26, 22 turns).

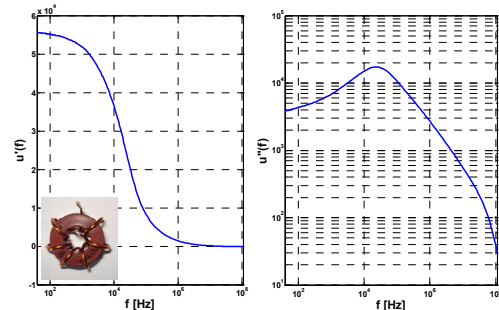


Fig. 8. The measured complex permeability for Vacuumschmelze Inc. VITROPERM 500F W380 core (see Table I) (left) real part (right) imaginary part.

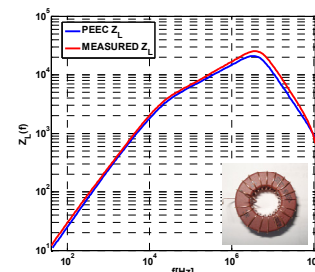


Fig. 9. Comparison of the impedance of the PEEC modeled inductor with the measurement (VITROPERM 500F W380, 20 turns).

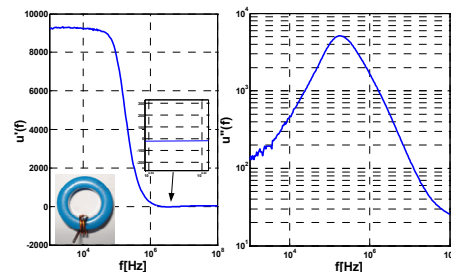


Fig. 10. The measured complex permeability for EPCOS ferrite T38 R 34 ring core (see Table I) (left) real part (right) imaginary part.

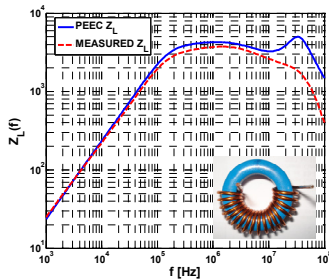


Fig. 11. Comparison of the impedance of the PEEC modeled inductor with the measurement (Ferrite T38 R 34, 20 turns).

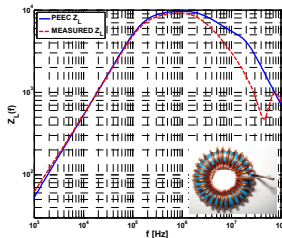


Fig. 12. Comparison of the impedance of the PEEC modeled inductor with the measurement (Ferrite T38 R 34, 30 turns).

#### REFERENCES

- [1] M. Hartmann, H. Ertl, and J. W. Kolar, "EMI Filter Design for High Switching Frequency Three-Phase/Level PWM Rectifier Systems", in *Proc. of the 25<sup>th</sup> Applied Power Electronic Conference*, Palm Springs, California, USA, Feb. 21-25, 2010, pp. 986-993.
- [2] M. L. Heldwein, *EMC Filtering for Three-Phase PWM Converters*, PhD thesis, ETHZ, 2008.
- [3] S. Wang, F. Lee, D. Chen, and W. Odendaal, "Effects of Parasitic Parameters on EMI Filter Performance," *IEEE Trans. Power Electron.*, vol. 19, no. 3, pp. 869-877, 2004.
- [4] R. West, "Common Mode Inductors for EMI Filters Require Careful Attention to Core Material Selection", *PCIM Magazine*, July 1995.
- [5] A. Muesing, M. L. Heldwein, T. Friedli, and J. W. Kolar, "Steps Towards Prediction of Conducted Emission Levels of an RB-IGBT Indirect Matrix Converter", in *Proc. of the Power Conversion Conference (PCC)*, Nagoya, Apr. 2-5, 2007, pp. 1181-1188.
- [6] A. E. Ruehli, "Equivalent Circuit Models for Three-Dimensional Multiconductor Systems", *IEEE Transactions on Microwave Theory and Techniques*, vol. 22, no. 3, pp. 216-221, 1974.
- [7] A. E. Ruehli and H. Heeb, "Circuit Models for Three-Dimensional Geometries Including Dielectrics," *IEEE Transactions on Microwave Theory and Techniques*, vol. 40, no. 7, pp. 1507-1516, 1992.
- [8] K. Pawluk and Z. Zycki, "Boundary-Integral Approach to Determine the Magnetic Field Created by a Permanent Magnet put in Free Space", *Int. Journal for Computation and Mathematics in Electrical and Electronic Engineering*, vol. 19, no.1, pp. 86-94, 2000.
- [9] G. Antonini, M. Sabatini, and G. Miscione, "PEEC Modeling of Linear Magnetic Materials", in *Proc. of IEEE International Symposium on Electromagnetic Compatibility*, Portland, Oregon, USA, Aug. 14-18, 2006, pp. 93-98.
- [10] J. P. Keradec, E. Clavel, J. P. Gonnet, V. Mazauric, "Introducing Linear Magnetic Materials in PEEC Simulations. Principles, Academic and Industrial Applications", in *Proc. of 40<sup>th</sup> Industry Applications Conf.*, Hong-Kong, Oct. 2-6, 2005, pp. 2236-2240.
- [11] H. Long, Z. Feng, H. Feng, A. Wang, "A Novel Accurate PEEC-Based 3D Modeling Technique for RF Devices of Arbitrary Conductor-Magnet Structure", *Microwave and Optical Technology Letters*, vol. 38, no. 3, pp. 237-240, June 2003.
- [12] E. Hoene, A. Lissner, S. Weber, S. Guttowski, W. John, and H. Reichl, "Simulating Electromagnetic Interactions in High Power Density Converters", in *Proc. of 36<sup>th</sup> Power Electronics Specialists Conf.*, Recife, Brazil, June 12-16, 2005, pp. 1665-1670.
- [13] T. De Oliveira, J.-L. Schanen, and J. M. Guichon, "PEEC-Models for EMC Filter Layout Optimisation", in *Proc. of the 6<sup>th</sup> Int. Conference on Integrated Power Electronics Systems (CIPS 2010)*, Nuremberg, Germany, March 16-18, 2010, Paper 13.3.
- [14] T. S. Tran., G. Meunier, P. Labie Y. Le Floch. J. Roudet, J. M. Guichon, and Y. Marechal, "Coupling PEEC-Finite Element Method for Solving Electromagnetic Problems", *IEEE Trans. on Magnetics*, vol. 44, no. 6, pp. 1330-1333, June, 2008.
- [15] D. M. Cook, *The Theory of the Electromagnetic Field*, 1975, Prentice-Hall, Inc., Englewood Cliffs, New Jersey, pp. 289-324.
- [16] M. Bartoli, A. Reatti, and M. K. Kazimierczuk, "Modeling of Iron-Powder Inductors at High Frequencies", in *Proc. of IEEE Industry Applications Society Annual Meeting*, Denver, USA, Oct. 2-6, 1994, pp. 1225-1232.
- [17] L. Dalessandro, W. G. H. Odendaal, and J. W. Kolar, "HF Characterization and Nonlinear Modeling of a Gapped Toroidal and Magnetic Structure", *IEEE Trans. on Power Electronics*, vol. 21, no. 5, pp. 1167-1175, Sept., 2006.
- [18] K. Zakrzewski and B. Tomczuk., "Magnetic Field Analysis and Leakage Inductance Calculation in Current Transformers by Means of 3-D Integral Methods", *IEEE Trans. on Magnetics*, vol. 32, no. 3, pp. 1637-1640, May 1996.
- [19] M. Lean and D. Bloomberg, "Nonlinear Boundary Element Method for 2D Magnetostatics", *Journal of Applied Physics*, vol. 55, no. 6, pp. 2195-2197, Mar., 1984.
- [20] T. Morisue, "A Consideration on the Computational Error of the Boundary Integral Equation Method for Magnetostatic Field Problems", *IEEE Trans. on Magnetics*, vol. 24, no. 6, pp. 2509-2511, Nov., 1988.
- [21] D. Gope, A. Ruehli, and V. Jandhyala, "Solving Low-Frequency EM-CKT Problems using the PEEC Method", *IEEE Trans. on Advanced Packaging*, vol. 30, no. 2, pp. 313-320, May, 2007.
- [22] Vacuumschmelze, Nanocrystalline VITROPERM - EMC Components, Vacuumschmelze GmbH. & Co., 2004
- [23] EPCOS, Ferrites and Accessories, EPCOS AG., 2006.
- [24] Micrometals Iron Powder Cores, "Power Conversion and Line Filter Application", *Issue L*, Feb. 2007.
- [25] D. Zhang, "Permeability Enhancement by Induced Displacement Current in Magnetic Material with High Permittivity", *Journal of Magnetism and Magnetic Materials*, vol. 313, no. 1, pp. 47-51, June, 2007.
- [26] R. Huang and D. Zhang, "Determination of Dimension-Independent Magnetic and Dielectric Properties for Mn-Zn Ferrite Cores and Its EMI Applications", *IEEE Transaction on Electromagnetic Compatibility*, vol. 50, no. 3, pp. 597-602, Aug., 2008.
- [27] J. P. Keradec, P. Fouassier, B. Cogitore, and F. Blache, "Accounting for Resistivity and Permittivity in High Frequency Permeability Measurements Application to MnZn Ferrites", in *Proc of 20th Instrument and Measurement Technology Conference (IMTC 2003)*, Vail, CO, USA, May 20-22, 2003, vol. 2, pp. 1252-1256.